IEEE Access
Multidisciplinary | Rapid Review | Open Access Journal

Received August 11, 2021, accepted September 1, 2021, date of publication September 10, 2021,
date of current version September 20, 2021.

Digital Object Identifier 10.1109/ACCESS.2021.3111759

Joint Delay and Phase Discriminator Based on ESPRIT for 5G NR Positioning

IVAN LAPIN[1], GONZALO SECO-GRANADOS[2], (Senior Member, IEEE), OLIVIER RENAUDIN[2], FRANCESCA ZANIER[1], AND LIONEL RIES[1]

[1]Radio Frequency Systems Division, European Space Agency, 2201 AZ Noordwijk, The Netherlands
[2]Department of Telecommunications and Systems Engineering, Universitat Autònoma de Barcelona, 08193 Bellaterra, Spain

Corresponding author: Ivan Lapin (ivan.lapin@esa.int)

This work was supported in part by the European Space Agency through the Networking Partnering Initiative (NPI) Program under Grant 4000123584/18/NL/MH, in part by the Secretariat of Universities and Research of the Enterprise and Knowledge Department of Generalitat of Catalonia through Beatriu de Pinós under Grant 2018 BP 0266, and in part by the H2020 Marie Skłodowska-Curie Co-funding of regional, national and international programmes (COFUND) under Contract 801370.

ABSTRACT A joint delay and phase discriminator based on the ESPRIT algorithm is proposed for positioning with the fifth generation (5G) New Radio (NR) downlink cellular signals. Since ESPRIT requires knowledge of the number of paths of the radio channel to operate, the proposed discriminator is coupled and studied with two channel order estimators: minimum descriptive length (MDL) and efficient channel order determination (ECOD). To mitigate the delay and phase outliers appearing when the MDL overestimates the channel order, a path selection criterion based on the signal-to-noise ratio (SNR) of the path is proposed. The ESPRIT discriminator is evaluated in terms of the distribution of the estimated channel order, and the delay and phase errors in the absence and presence of multipath. It is observed that the path selection criterion makes the MDL suitable for positioning as no delay and phase outliers are produced. In the presence of multipath, the ESPRIT discriminator achieves lower mean and root-mean-square delay and phase errors than the commonly used early-minus-late power (EMLP) and 2-argument arctangent (ATAN2) discriminators.

INDEX TERMS 5G new radio, cellular positioning, channel order estimation, delay and phase discriminator, ESPRIT.

I. INTRODUCTION

The fourth generation (4G) Long-term Evolution (LTE) and fifth generation (5G) New Radio (NR) cellular systems have evolved to become a relevant source of positioning thanks to their favorable signal characteristics and good coverage in urban environments [1]. Positioning with cellular signals is of particular interest to the users of the Global Navigation Satellite System (GNSS) who may experience reduced performance in challenging environments such as in urban canyons or indoors [2]. The integration of the cellular downlink delay measurements with GNSS allows to improve the availability, continuity, accuracy, and integrity positioning performances [3]–[7]. To further improve positioning performances, the signal phase measurements representing the carrier phase can also be obtained from the received signal and included in the navigation processing [8].

Downlink delay and phase measurements can be obtained by tracking the pilots of the transmitted cellular signals. LTE and 5G NR waveforms utilize the orthogonal frequency division multiplexing (OFDM) scheme and contain signals for various purposes including channel estimation, positioning, and time/frequency synchronization [9], [10]. Although the cellular base stations can transmit a dedicated positioning signal called the positioning reference signal (PRS), it has not been widely adopted in LTE, and the extent of its utilization in 5G NR is still uncertain. Instead of the PRS, other downlink signals can be exploited for positioning, some of which do not require the user subscription or specific network configuration. One such signal in LTE systems, called the cell-specific reference signal (CRS), has been shown to provide satisfactory performance for ranging purposes [11], [12]. In 5G NR systems, the CRS is no longer present and is replaced by other reference signals such as the channel state information reference signal (CSI-RS) [13]. For potential downlink positioning in the frequency range 1 (FR1), the CSI-RS configured as the tracking reference signal (TRS) is further considered. The TRS is nominally used for fine synchronization and channel analysis for the user equipment (UE). Although the CSI-RS is UE-dependent, the considered configuration has a high

The associate editor coordinating the review of this manuscript and approving it for publication was Venkata Ratnam Devanaboyina.

subcarrier density making it suitable for the evaluation of the delay estimation and positioning.

The receiver obtains the delay and phase measurements by continuously tracking the received signal. In terrestrial scenarios, the effects contributing to the delay and phase measurements include the geometrical distance between the transmitter and receiver, transmitter and receiver clocks, and various instrumental delays in the signal processing chain. The signal tracking is typically performed by a closed-loop architecture, where the tracking loops continuously update the delay and phase estimates. The tracking loops utilize so-called discriminators whose outputs they drive to zero by employing a feedback loop to the received signal. The discriminators may introduce additional biases and errors to the measurements due to the multipath and noise. The delays are estimated to the subsample accuracy as depending on the sampling rate, a single sample may represent a positioning error equal to several meters. The early-minus-late (EML) delay discriminator was proposed by Yang *et al.* [14] in the frequency domain for an arbitrary OFDM waveform and fixed correlator spacing of half a sample. The EML power (EMLP) delay discriminator was studied by Serant *et al.* [15] in the time domain for an arbitrary correlator spacing and terrestrial digital video broadcast OFDM signals. The work was expanded into the frequency domain by Chen *et al.* [16]. A phase discriminator based on the 2-argument arctangent (ATAN2) operator applied to the channel frequency response (CFR) estimated using the reference pilots was proposed by del Peral *et al.* [17] for LTE positioning and further expanded in the work of Shamaei and Kassas [18]. Positioning of an airborne drone receiver implementing delay and phase ranging using the EMLP and ATAN2 discriminators was demonstrated in real flight scenarios [8].

Although the EMLP and ATAN2 discriminators approach closely the performance of the maximum-likelihood estimator in the additive white Gaussian noise (AWGN) channel, they experience degraded performances in multipath channels that introduce additional biases to the delay and phase estimates. The multipath channels are typically experienced in urban environments, where achieving the maximum benefit of cellular positioning is desired due to the limited visibility of GNSS satellites. Delay estimators robust to multipath are based on super-resolution algorithms (SRAs). Various SRAs were studied for indoor positioning by Li and Pahlavan [19]. The ESPRIT algorithm was used as a delay estimator coupled with a Kalman filter for positioning with LTE signals [20], [21]. Due to its wide estimation range, the ESPRIT algorithm was also used for the signal acquisition in LTE positioning [8], [18]. A joint delay and phase estimation using ESPRIT was proposed by Dun *et al.* [22]. Using the ESPRIT algorithm as a joint delay and phase discriminator that can be implemented in a tracking loop has not yet been investigated.

The ESPRIT algorithm requires knowledge of the number of paths of the radio channel to operate. As the true number of paths is unknown, the estimation of the channel order in multipath environments is needed. The most recognized channel order estimator is the minimum descriptive length (MDL) method [23]. The MDL is based on information-theoretic criteria and has been widely adopted for positioning with SRA algorithms [18], [19], [21]. However, the MDL may overestimate the channel order that can cause ESPRIT to produce delay outliers in the form of false paths arriving before the true earliest path [18], [21], [24]. The overestimation may occur even for a high signal-to-noise ratio (SNR) [25]. To avoid the overestimation, different channel order methods may be used. Lavias *et al.* [26] proposed the efficient channel order determination (ECOD) method that is based on eigenvalue differencing and does not overestimate the channel in sufficiently high SNR. For positioning, Driusso *et al.* [20] addressed the effect of the MDL overestimation on ESPRIT by applying a threshold to the delay measurements. The utilization of the ECOD and the study of alternative ways to select the true earliest path during the overestimation remain unexplored topics in the context of cellular positioning.

In this paper, a joint delay and phase discriminator based on the ESPRIT algorithm is proposed for positioning with 5G NR cellular signals. The main contributions of the paper are summarized as follows:

(i) A waveform suitable for the performance evaluation of delay and phase discriminators in 5G NR systems is proposed.
(ii) A discriminator based on ESPRIT capable of joint delay and phase error estimation suitable for the signal tracking loops is proposed.
(iii) The impact of the channel order overestimation of the MDL method on the ESPRIT algorithm is investigated. A path selection criterion based on the SNR of the path is proposed.
(iv) The ESPRIT discriminator is coupled with the MDL and ECOD methods, and the resulting combinations are compared in terms of the distribution of the estimated channel order, and the delay and phase errors in the absence and presence of multipath.

The remainder of the paper is organized as follows. Section II proposes the 5G NR downlink waveform for positioning evaluation. Section III defines the commonly used EMLP and ATAN2 discriminators. Section IV proposes the join delay and phase discriminator based on ESPRIT. The results of the performance evaluation of various delay and phase discriminators are presented in Section V. Conclusions are given in Section VI.

Notation: Matrices are denoted as uppercase boldface letters, such as $\mathbf{X} \in \mathbb{C}^{M\times N}$. Column vectors are denoted as lowercase boldface letters, such as $\mathbf{x} \in \mathbb{C}^{M\times 1}$. $\mathbf{I}_{P\times P}$ is a $P \times P$ eye matrix, $\mathbf{0}_{P\times Q}$ is a $P \times Q$ zero matrix, and $\mathbf{0}_{P\times 1}$ is a zero column vector of length P. The operators $(\cdot)^T$, $(\cdot)^H$, $(\cdot)^{-1}$, and $(\cdot)^\dagger$ denote the transpose, the Hermitian transpose, the inverse, and the Moore–Penrose pseudoinverse of a matrix, respectively. $|\cdot|$, $\angle(\cdot)$, and $(\cdot)^*$ denote the absolute value, the argument, and the conjugate of a complex

number, respectively. The operator min (**x**) denotes the minimum value of a vector **x**. The operator sort (**x**) produces a vector whose values are sorted in ascending order.

II. CELLULAR DOWNLINK WAVEFORMS FOR POSITIONING EVALUATION

The 5G NR and LTE cellular downlink waveforms are based on the OFDM transmission scheme that is described by a time-frequency grid in which a symbol time index i and frequency subcarrier index n uniquely identify a single transmitted complex data symbol. A digital baseband signal $x_i[l]$ of the i-th OFDM symbol is expressed as

$$x_i[l] = \frac{1}{N_{\text{fft}}} \sum_{n=-\frac{N_{\text{fft}}}{2}}^{\frac{N_{\text{fft}}}{2}-1} X_i[n] \cdot e^{j\frac{2\pi}{N_{\text{fft}}} n (l-N_{\text{cp}})}, \tag{1}$$

for $l = 0, 1, \ldots, N_{\text{fft}} + N_{\text{cp}} - 1$, where n is the OFDM subcarrier index, $X_i[n]$ is the complex data symbol transmitted on the n-th subcarrier, N_{fft} is the total number of subcarriers available for modulation that are symmetrically arranged around the direct current (DC) component with the index $n = 0$, and N_{cp} is the number of samples within the cyclic prefix (CP). The CP is a sequence of the last N_{cp} samples of the symbol prepended to its beginning to provide a guard interval preventing the inter-symbol interference from the previous symbol whilst allowing for a circular convolution of the channel. The digital signal in (1) can be conveniently generated using the inverse fast Fourier transform (IFFT). The continuous signal is then generated using the digital-to-analog converter. The resulting subcarrier spacing is $\Delta f = \frac{1}{T_s}$ [Hz], where T_s [s] is the duration of the OFDM symbol without the CP.

The 3GPP specification maps the $N_{\text{sc}} \leq N_{\text{fft}}$ transmitted resource elements to the N_{fft} available subcarriers. The OFDM subcarrier index n on which the k-th resource element is transmitted can be obtained using the mapping function $\kappa(k)$ as

$$n = \kappa(k) = \begin{cases} k - \dfrac{N_{\text{sc}}}{2} & \text{when } k < \frac{N_{\text{sc}}}{2}, \\ k - \dfrac{N_{\text{sc}}}{2} + \xi & \text{otherwise,} \end{cases} \tag{2}$$

for $k = 0, 1, \ldots, N_{\text{sc}} - 1$, where $\xi \in \{0, 1\}$ reflects whether the DC component is used for transmission or not. The unused subcarriers are left empty.

The 5G NR and LTE waveforms may contain various signals that can be exploited for positioning. Although a dedicated positioning signal called the PRS exists in the 3GPP specifications, it is not considered for the positioning evaluation in this paper as the extent of its utilization in 5G NR is still uncertain.

A. 5G NR DOWNLINK EVALUATION WAVEFORM

The 5G NR OFDM transmission scheme is logically organized into 10 ms long radio frames. The radio frame is composed of $10 \cdot 2^{\mu}$ slots, where $\mu \in \{0, 1, 2, 3, 4\}$ is called the numerology parameter whose value is driven by the frequency band and the signal bandwidth [9]. In the normal CP mode, the slot is composed of $N_{\text{symb}}^{\text{DL}} = 14$ symbols. The smallest logical block of the OFDM grid is called the resource block (RB) and comprises $N_{\text{RB}}^{\text{DL}} = 12$ subcarriers and $N_{\text{symb}}^{\text{DL}}$ symbols. The subcarriers are spaced $\Delta f_{\text{sc}} = 15 \cdot 2^{\mu}$ kHz apart. The DC component is used for data transmission and $\xi = 0$ in (2).

To assign values to different parameters and allow for the evaluation of positioning performances using reference pilots, a potential 5G NR downlink waveform that is not necessarily linked to any particular deployment or specification is proposed. The waveform is configured to the maximum allowable transmission bandwidth of $B = 100$ MHz in the FR1, time division duplexing (TDD) scheme, normal CP mode, numerology $\mu = 1$, and cell ID 42 [27]. In this configuration, the radio frame is composed of 20 slots and the subcarrier spacing is $\Delta f_{\text{sc}} = 30$ kHz. The length of the FFT/IFFT is $N_{\text{fft}} = 4096$ resulting in the sampling frequency $f_s = N_{\text{fft}}\, \Delta f_{\text{sc}} = 122.88$ Msps. After the guard band removal, the number of RBs used for transmission is $N_{\text{sc}}^{\text{RB}} = 273$. The TDD mode is configured to the slot format 32 that reserves the first ten symbols of the slot for the downlink and the last two symbols for the uplink whilst the remaining two slots are left empty [28]. The values of the relevant parameters are summarized in Table 1.

Although being UE-dependent, the CSI-RS is used for signal tracking and positioning in the proposed 5G NR evaluation waveform. The CSI-RS is configured as the TRS resulting in its periodic transmission every slot, frequency density of $\rho = 3$ pilots per RB, full occupation of the 273 available RBs for the UE, and no code division multiplexing [9]. The assumed configuration provides $P = N_{\text{sc}}^{\text{RB}}\, \rho = 273 \cdot 3 = 819$ pilots spanning the full bandwidth and is considered relevant for the evaluation of positioning performances as it maximizes the presence of the pilots. The subcarrier spacing between adjacent pilots is $\Delta P = \frac{N_{\text{RB}}^{\text{DL}}}{\rho} = \frac{12}{3} = 4$. The initial position of the first CSI-RS pilot is for convenience configured with the time offset $l_0 = 0$ and the subcarrier offset $k_0 = 0$. The distribution of the CSI-RS pilots assumed in the 5G NR waveform is shown in Fig. 1a. The downlink symbols are considered to be fully occupied by the physical downlink shared channel (PDSCH) that is simulated by a random data generator. No data transfer is present on the uplink channel.

B. LTE DOWNLINK EVALUATION WAVEFORM

For comparison with 5G NR, an LTE downlink evaluation waveform is also considered. The OFDM scheme of LTE systems can be interpreted as a subset of the 5G NR scheme configured with $\mu = 0$ [10]. A notable difference is a smaller maximum transmission bandwidth of $B = 20$ MHz and frequency division duplexing (FDD) scheme that is used in the deployments on the European continent [29]. On the

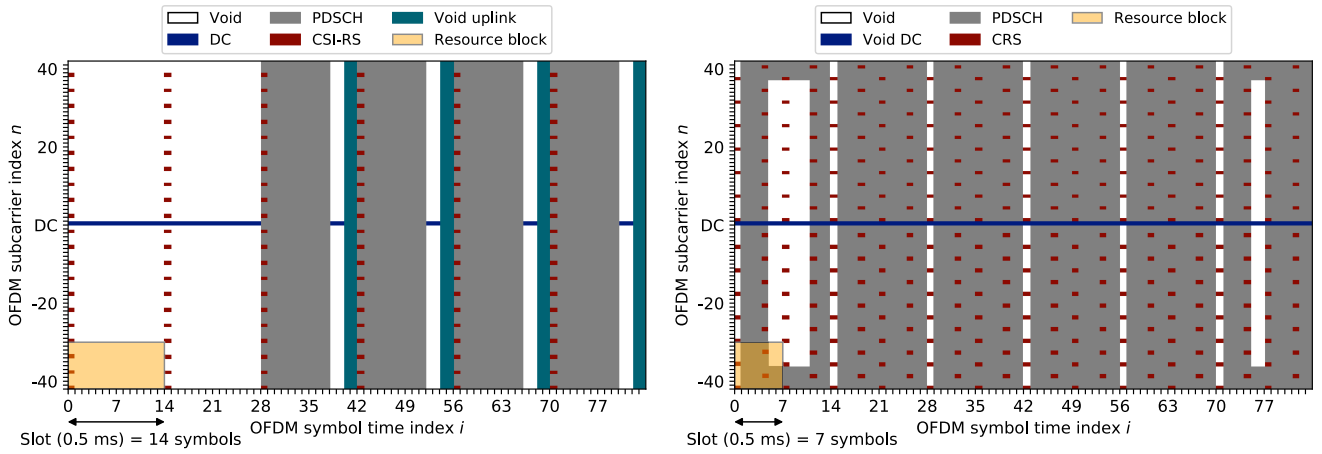

FIGURE 1. Signals assumed in the first 84 symbols and central 84 subcarriers of the (a) 5G NR evaluation waveform and (b) LTE evaluation waveform. The DC components, resource blocks, and slot durations are also shown in the figure.

TABLE 1. Parameters of the 5G NR and LTE evaluation downlink waveforms assumed in the study.

System	5G NR	LTE
Frequency range	FR1	FR1
Bandwidth B [MHz]	100	20
Duplexing mode	TDD	FDD
Cyclic prefix mode	Normal	Normal
Numerology μ	1	-
Subcarrier spacing Δf_{sc} [kHZ]	30	15
Slots per radio frame	20	20
Symbols per slot $N_{\text{symb}}^{\text{DL}}$	14	7
Symbol duration without CP T_{s} [μs]	33.33	66.67
FFT Size N_{fft}	4096	2048
Sampling frequency f_{s} [Msps]	122.88	30.72
Number of resource blocks $N_{\text{sc}}^{\text{RB}}$	273	100
Transmission on the DC component	Yes	No
Cell ID	42	42
Tracked reference pilots	CSI-RS	CRS
Pilot subcarrier spacing ΔP	4	6
Number of pilots per bandwidth P	819	200

contrary to 5G NR systems, the DC component is omitted from transmission in LTE and $\xi = 1$ in (2). The parameters of the proposed LTE waveform are summarized in Table 1. To allow the UE to perform coherent demodulation and to estimate the quality of the downlink channel, the CRS pilots are transmitted in the downlink waveform. The configuration of the CRS is only driven by the cell ID and the antenna port. The distribution of the CRS pilots assumed in the LTE waveform is for the first antenna port of the cell ID 42 shown in Fig. 1b.

III. DELAY AND PHASE DISCRIMINATORS

Delay and phase discriminators allow for continuous signal tracking in the closed-loop receiver architecture as they estimate the delay and phase offsets between the received signal and the locally generated replica. The block diagram of the signal tracking stage of a typical OFDM positioning receiver implementing the delay and phase discriminators is shown in Fig. 2. In the tracking stage, the receiver updates the delay and phase estimates with the output of the tracking loops. To drive the outputs of the discriminators to zero and maintain the lock of the signal, the delay and phase estimates are fed back to the demodulation block in the next receiver iteration to remove the estimated offsets from the received signal. The delays are estimated to the subsample accuracy and removed from the input signal at the integer and fractional parts. The signal tracking stage is preceded by the signal acquisition stage that initializes the delay and phase estimates. The signal acquisition is for simplicity omitted from the block diagram shown in Fig. 2 as it does not involve the discriminators.

The relation between the received signal and the local replica at the receiver is expressed by the CFR that can be estimated from the pilots in the OFDM waveform as

$$\hat{h}_i(p) = \hat{\Upsilon}_{i,p} \Upsilon_{i,p}^*, \tag{3}$$

where p is the pilot index, i is the symbol time index, $\hat{\Upsilon}_{i,p}$ is the received pilot symbol with the removed delay and phase estimates from the previous iteration of the tracking loops as shown in Fig. 2, and $\Upsilon_{i,p}$ is the pilot symbol replica at the receiver. The pilot index $p = 0, 1, \ldots, P-1$ is assigned to each of the $P \leq N_{\text{sc}}$ pilots of a given reference signal. For equally spaced pilots with a constant transmission pattern, the OFDM index n_p of the p-th pilot can be expressed as

$$n_p = \kappa \left(p \, \Delta P + k_0 \right), \tag{4}$$

where ΔP is the pilot spacing, k_0 is the subcarrier offset of the first pilot from the first subcarrier used for transmission, and $\kappa(k)$ is the mapping function in (2). Considering the pilot spacing and number of the pilots are the same for all

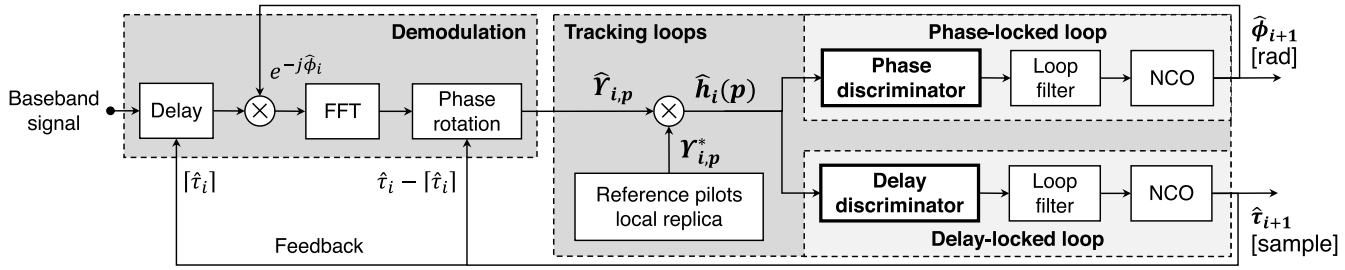

FIGURE 2. Block diagram of the signal tracking stage of a typical closed-loop OFDM positioning receiver. The receiver tracks the input signal using the tracking loops comprising of discriminators, loop filters, and numerically controlled oscillators (NCO). The tracking loops keep updating the code and phase estimates, which are then fed back to the demodulation block and removed from the received signal in the next receiver iteration to maintain the lock of the signal. The integer part of the delay estimate ($\lceil\hat{\tau}\rceil$) is used to shift the FFT window in the time domain and the fractional part ($\hat{\tau} - \lceil\hat{\tau}\rceil$) is applied as a phase rotation of the subcarriers in the frequency domain. The traditionally used EMLP delay and ATAN2 phase discriminators are proposed to be replaced by the ESPRIT discriminator that provides both estimates.

symbols containing the CSI-RS pilots in the 5G NR downlink evaluation waveform from Section II-A, the symbol time index i is for simplicity omitted for the remainder of this section.

A. EARLY-MINUS-LATE POWER DELAY DISCRIMINATOR

The EMLP delay discriminator estimates the delay offset by correlating the received signal with the local replica at the receiver. The replica is delayed and advanced by $\pm\delta$ samples and the resulting two correlators are referred to as the early and late branches. The time shift property of the discrete Fourier transform $\mathcal{F}\left(x(l\,T_\mathrm{s} \pm \tau)\right) = X[n]\,e^{\pm j\frac{2\pi}{N_\mathrm{fft}}n\,\tau}$ allows to define the correlator branches in the frequency domain as phase rotations of the OFDM subcarriers. A delay offset e_τ of the received signal causes additional rotation and can be expressed at a given time symbol as [14]

$$R\left(e_\tau, \mp\delta\right) = \frac{1}{P}\sum_{p=0}^{P-1}\hat{h}(p)\,e^{-j\frac{2\pi}{N_\mathrm{fft}}(e_\tau \pm \delta)n_p}, \tag{5}$$

where $R\left(e_\tau, -\delta\right)$ represents the output of the early branch, $R\left(e_\tau, +\delta\right)$ represents the output of the late branch, P is the number of pilots, and n_p is the OFDM index of the pilot from (4). The power of the received pilot from (3) is assumed to be equal on each subcarrier and can be denoted as $|\hat{\Upsilon}_p|^2 = C$. The power of each pilot replica at the receiver is assumed to be unitary and simplifies to $|\Upsilon_p|^2 = 1$. The normalized non-coherent EMLP delay discriminator is then defined as

$$D_\mathrm{EMLP}\left(e_\tau, \delta\right) = \frac{|R\left(e_\tau, -\delta\right)|^2 - |R\left(e_\tau, \delta\right)|^2}{C\,k_\mathrm{EMLP}\left(\delta\right)}\ [\mathrm{sample}], \tag{6}$$

where the unit of samples denotes the estimated delay offset as a fractional number of samples that can be converted to the unit of seconds by dividing it with the signal sampling frequency f_s, and $k_\mathrm{EMLP}\left(\delta\right)$ is the normalization factor to keep $D_\mathrm{EMLP}\left(e_\tau, \delta\right) \approx e_\tau$ when $e_\tau \approx 0$. The normalization factor can be expressed for an arbitrary correlator spacing as [16]

$$k_\mathrm{EMLP}\left(\delta\right) = \frac{2\left[1 - \delta\pi\beta\,\sin\left(2\pi\beta\delta\right) - \cos\left(2\pi\beta\delta\right)\right]}{\left(\pi\beta\right)^2\,\delta^3}, \tag{7}$$

where $\beta = \frac{P\,\Delta P}{N_\mathrm{fft}}$ is the OFDM waveform factor that corresponds to the ratio between the usable signal bandwidth spanned by the pilots and the IFFT/FFT length.

1) DELAY ERROR VARIANCE

In the AWGN channel without multipath, the linear region of the EMLP discriminator function in (6) approximates to $D_\mathrm{EMLP}\left(e_\tau, \delta\right) \approx e_\tau + n_{e_\tau}$, where n_{e_τ} is approximately the zero-mean white complex Gaussian noise with the variance $\sigma^2_{e_\tau}$ that can be expressed as [15]

$$\sigma^2_{e_\tau} = \frac{4\left(1 - \mathrm{sinc}\left(2\pi\beta\delta\right)\right)\mathrm{sinc}^2\left(\pi\beta\delta\right)}{P\,\mathrm{SNR}\,k^2_\mathrm{EMLP}\left(\delta\right)} \cdot\left(1 + \frac{\left(1 + \mathrm{sinc}\left(2\pi\beta\delta\right)\right)}{2\,P\,\mathrm{SNR}\,\mathrm{sinc}^2\left(\pi\beta\delta\right)}\right), \tag{8}$$

where the SNR is defined as

$$\mathrm{SNR} = \frac{S}{\sigma^2_\mathrm{n}} = \frac{C}{w^2}, \tag{9}$$

where S is the power of the signal over N_sc subcarriers, σ^2_n is the power of the noise over N_sc subcarriers, and w^2 is the power of the noise over a single subcarrier. The expected performance in the multipath-free AWGN channel is relevant to understand the impact of the signal parameters on the lower bound of the discriminator error.

2) CRAMÉR–RAO LOWER BOUND

The Cramér–Rao lower bound (CRLB) describes the minimum achievable variance of an unbiased estimator in sufficiently high SNR and is defined for an arbitrary OFDM delay estimator in the AWGN channel without multipath as [30]

$$\mathrm{CRLB} = \frac{N^2_\mathrm{fft}}{8\pi^2\,\mathrm{SNR}\sum_{p=0}^{P-1}n_p^2}\ [\mathrm{sample}^2], \tag{10}$$

where n_p is the OFDM index of the pilot from (4).

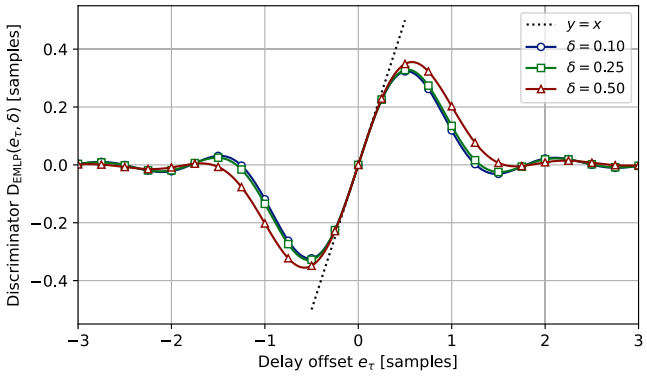

FIGURE 3. EMLP discriminator function of the 5G NR downlink evaluation waveform for various values of the correlator spacing δ. The linear region with the unit slope ($y = x$) is also shown.

3) DELAY TRACKING THRESHOLD

The tracking threshold determines the maximum delay offset that can still be tracked by the discriminator. Delay offsets above this threshold will likely cause the tracking loop to lose the lock of the signal. In the case of the EMLP discriminator, it is defined as the delay offset whose deviation from the ideal linearity does not exceed a given threshold α as

$$\zeta_{\text{EMLP}} = \underset{e_\tau}{\text{argmax}}\{|D_{\text{EMLP}}(e_\tau, \delta) - e_\tau| \leq \alpha\}. \tag{11}$$

As a rule of thumb, the value ζ_{EMLP} determines the maximum acceptable 3-sigma of the total jitter and dynamic stress error of a delay-locked loop (DLL) implementing the EMLP discriminator ($3\,\sigma_{\text{DLL}} \leq \zeta_{\text{EMLP}}$) [2]. To enable the analytical evaluation of the EMLP discriminator function, the non-coherent early and late branch outputs of the EMLP discriminator can be approximated for large FFT sizes $N_{\text{fft}} \gg 1$ in a noiseless multipath-free channel as [16]

$$|R(e_\tau, \pm\delta)|^2 \approx C\,\text{sinc}^2(\pi\beta(e_\tau \pm \delta)), \tag{12}$$

where $\text{sinc}(x) = \frac{\sin(x)}{x}$. By substituting (12) into (6), the closed-form expression of the discriminator function becomes

$$D_{\text{EMLP}}(e_\tau, \delta) \approx \frac{\text{sinc}^2(\pi\beta(e_\tau - \delta)) - \text{sinc}^2(\pi\beta(e_\tau + \delta))}{k_{\text{EMLP}}(\delta)}. \tag{13}$$

The function of the EMLP discriminator (13) evaluated under various correlator spacings is shown in Fig. 3. The shape of the discriminator function gives a name to the so-called S-curve. Outside the linear region, the discriminator output no longer corresponds to the delay offset and the performance of the tracking loop degrades. Fig. 3 shows that the correlator spacing has a negligible impact on the shape of the discriminator function around the linear region.

B. ATAN2 PHASE DISCRIMINATOR

The phase discriminator function estimates the phase offset between the received signal and the local replica at the receiver by applying the ATAN2 operator to the estimated CFR and can be expressed as [17], [18]

$$D_{\text{ATAN2}} = \angle\left(\sum_{p=0}^{P-1}\hat{h}(p)\right)\ [\text{rad}]. \tag{14}$$

1) PHASE ERROR VARIANCE

In the AWGN channel without multipath, the ATAN2 discriminator function becomes $D_{\text{ATAN2}} = e_\phi + n_{e_\phi}$, where n_{e_ϕ} is approximately the zero-mean white complex Gaussian noise with the variance $\sigma^2_{e_\phi}$ that can be expressed as [18]

$$\sigma^2_{e_\phi} = \frac{1}{2\,P\,\text{SNR}}\left(1 + \frac{1}{2\,P\,\text{SNR}}\right)\ [\text{rad}^2]. \tag{15}$$

2) PHASE TRACKING THRESHOLD

The ATAN2 tracking threshold is limited by the 2π pull-in range of the argument operator used in (14). As a conservative rule of thumb, the tracking threshold ζ_{ATAN2} determines the maximum acceptable 3-sigma of the total jitter and dynamic stress error of a phase-locked loop (PLL) implementing the ATAN2 discriminator ($3\,\sigma_{\text{PLL}} \leq \zeta_{\text{ATAN2}}$) [2]. The threshold is set to one-fourth of the pull-in range of the ATAN2 discriminator resulting in

$$\zeta_{\text{ATAN2}} = \frac{\pi}{2}\ [\text{rad}]. \tag{16}$$

IV. JOINT DELAY AND PHASE DISCRIMINATOR BASED ON ESPRIT

The ESPRIT algorithm is commonly used to estimate directly delays and phases of paths in the radio channel during the signal acquisition [18]. In this section, the use of ESPRIT as a discriminator replacing the traditionally used EMLP and ATAN2 discriminators is proposed. At the input, the algorithm takes the CFR with the removed delay and phase estimates from the previous iteration of the tracking loops as shown in Fig. 2.

Although the remainder of the section assumes that the line-of-sight (LOS) component is always present in the radio channel, this assumption does not invalidate the usability of ESPRIT in the non-LOS conditions. In the case the LOS is not present or is lost, the ESPRIT algorithm will naturally track the first arriving multipath component. The decision on whether the receiver is tracking the LOS or non-LOS is usually taken by the navigation processor and is beyond the scope of this paper.

A. DELAY OFFSET ESTIMATION

The ESPRIT discriminator estimates the delay offsets of paths using the rotational invariance property of the estimated CFR at the receiver. Assuming P received pilots at a given time symbol, the CFR $\hat{\mathbf{h}}$ can be expressed as

$$\hat{\mathbf{h}} = [\hat{h}(0),\ \hat{h}(1), \ldots,\ \hat{h}(P-1)]^T \in \mathbb{C}^{P\times 1}, \tag{17}$$

where $\hat{h}(p)$ is the CFR from (3). The CFR can be organized into snapshot vectors $\mathbf{x}(q)$ of length M as

$$\mathbf{x}(q) = [\hat{h}(q),\ \hat{h}(q+1), \ldots,\ \hat{h}(q+M-1)]^T \in \mathbb{C}^{M\times 1}, \tag{18}$$

where $M \leq P$. The parameter $m \in [0,1]$ is a design parameter of the ESPRIT discriminator that determines the length of snapshots $M = \lfloor m \cdot P \rfloor$. Higher values of m increase the multipath resolution at the cost of reduced noise averaging. The configuration of this parameter should consider the number of expected paths in the channel, denoted as L, as it is necessary that $M \geq L$. The number of snapshots is determined as $N = P - M$. The data matrix $\mathbf{X}$ can be constructed as

$$\mathbf{X} = [\mathbf{x}(0),\ \mathbf{x}(1), \ldots,\ \mathbf{x}(N-1)]^T \in \mathbb{C}^{M\times N}. \tag{19}$$

The singular value decomposition (SVD) of $\mathbf{X}$ is

$$\mathbf{X} = \mathbf{U}\,\mathbf{\Sigma}\,\mathbf{V}^H, \tag{20}$$

where $\mathbf{U} \in \mathbb{C}^{M\times M}$ and $\mathbf{V} \in \mathbb{C}^{N\times N}$ are unitary matrices and $\mathbf{\Sigma} \in \mathbb{C}^{M\times N}$ is a diagonal matrix containing singular values

$$\text{diag}\left(\hat{\mathbf{\Sigma}}\right) = [\sigma_0, \sigma_1, \ldots, \sigma_{\min([M,N])}]^T, \tag{21}$$

where $\sigma_j \geq \sigma_{j+1}$. The standard ESPRIT approach can be used to estimate the delays of L paths from the snapshot matrix $\mathbf{X}$. The ESPRIT discriminator steps are defined as follows:

Step 1: Extract the signal column subspace as

$$\mathbf{U}_\text{s} = \mathbf{U} \cdot [\mathbf{I}_{L\times L}\mathbf{0}_{L\times(M-L)}]^T \in \mathbb{C}^{M\times L}. \tag{22}$$

Step 2: Split $\mathbf{U}_\text{s}$ into two sub-matrices defined as

$$\mathbf{U}_1 = [\mathbf{I}_{(M-1)\times(M-1)}\mathbf{0}_{(M-1)\times 1}] \cdot \mathbf{U}_\text{s} \in \mathbb{C}^{(M-1)\times L}, \tag{23}$$
$$\mathbf{U}_2 = [\mathbf{0}_{(M-1)\times 1}\mathbf{I}_{(M-1)\times(M-1)}] \cdot \mathbf{U}_\text{s} \in \mathbb{C}^{(M-1)\times L}. \tag{24}$$

Step 3: Estimate the ESPRIT rotational matrix as

$$\mathbf{\Psi} = \mathbf{U}_1^\dagger \mathbf{U}_2 \in \mathbb{C}^{L\times L}. \tag{25}$$

Step 4: Compute the eigenvalues ψ_l of $\mathbf{\Psi}$ and their complex arguments as

$$\boldsymbol{\psi} = [\angle(\psi_0), \angle(\psi_1), \ldots, \angle(\psi_{L-1})]^T \in \mathbb{C}^{L\times 1}\ [\text{rad}]. \tag{26}$$

Step 5: Compute the delays of the paths and sort them in ascending order as

$$\hat{\boldsymbol{\tau}} = \text{sort}\left(-\frac{\boldsymbol{\psi}}{2\pi\,\Delta P \Delta f_{sc}}\right) = [\hat{\tau}_0,\ \hat{\tau}_1, \ldots, \hat{\tau}_{L-1}]^T \in \mathbb{C}^{L\times 1}\ [s]. \tag{27}$$

It is noted that the index l of $\hat{\tau}_l$ from (27) does not necessarily identify the same path as the index of ψ_l from (26) due to the sorting operation between steps 4 and 5.

The ESPRIT discriminator takes the delay of the earliest path as the estimated delay offset as $D^{(\tau)}_\text{ESPRIT} = \hat{\tau}_0$. The ESPRIT delay tracking threshold is limited by the range of the argument operator $\angle(\psi_l) \in (-\pi, \pi]$ from (26) and constrains the delay offset estimation to

$$-\zeta_\text{ESPRIT} \leq e_\tau < \zeta_\text{ESPRIT}\ [\text{s}], \tag{28}$$

where $\zeta_\text{ESPRIT} = \frac{1}{2\,\Delta P\,\Delta f_\text{sc}}$ is the delay tracking threshold.

B. PHASE OFFSET ESTIMATION

To estimate the phase offsets, the complex amplitudes of paths need to be determined from the CFR. In the AWGN channel without multipath, the CFR at a given time symbol can be expressed as

$$\mathbf{h} = \mathbf{G}\mathbf{\Lambda} + \mathbf{w}, \tag{29}$$

where $\mathbf{\Lambda} = [\Lambda_o, \Lambda_1 \ldots, \Lambda_{L-1}]^T \in \mathbb{C}^{L\times 1}$ are the complex amplitudes of the paths, $\mathbf{w} \in \mathbb{C}^{P\times 1}$ is the additional zero-mean complex Gaussian noise, and $\mathbf{G} \in \mathbb{C}^{P\times L}$ is the delay matrix defined as

$$\mathbf{G} = \exp\left(-j\frac{2\pi f_\text{s}}{N_\text{fft}}\,\boldsymbol{\tau}\,[n_0, \ldots, n_{P-1}]\right)^T \in \mathbb{C}^{P\times L}, \tag{30}$$

where n_p is the OFDM index of the pilot from (4). The estimated delay matrix $\hat{\mathbf{G}}$ is obtained by substituting (27) into (30). The complex amplitudes can then be estimated using the least-squares solution as

$$\hat{\mathbf{\Lambda}} = \left(\hat{\mathbf{G}}^H\hat{\mathbf{G}}\right)^{-1}\hat{\mathbf{G}}^H\hat{\mathbf{h}} \in \mathbb{C}^{L\times 1}. \tag{31}$$

The phase of the l-th path can be determined as

$$\hat{\phi}_l = \angle\left(\hat{\Lambda}_l\right)\ [\text{rad}]. \tag{32}$$

The ESPRIT discriminator takes the phase of the earliest path as the estimated phase offset as $D^{(\phi)}_\text{ESPRIT} = \hat{\phi}_0$. The phase tracking threshold of ESPRIT is the same as that of the ATAN2 discriminator from Section III-B2.

C. CHANNEL ORDER ESTIMATION

To properly estimate the delay and phase offsets in multipath environments, the ESPRIT algorithm requires knowledge of the channel order L. Channel order estimators usually rely on the information included in the eigenvalues $\lambda_0 \geq \lambda_1 \geq \ldots \geq \lambda_{M-1}$ of the autocorrelation matrix obtained from the data matrix as $\hat{\mathbf{R}}_x = \frac{1}{N}\mathbf{X}\mathbf{X}^H \in \mathbb{C}^{M\times M}$. The eigenvalues can be more conveniently determined from the singular values in (21) as $\lambda_j = \frac{\sigma_j^2}{N}$.

1) MINIMUM DESCRIPTIVE LENGTH METHOD

The MDL method is based on the information-theoretic criteria and can be computed as [23]

$$\text{MDL}(l) = -N(M-l)\ln\left[\frac{\prod_{j=l}^{M-1}\lambda_j^{\frac{1}{M-l}}}{\frac{1}{M-l}\sum_{j=l}^{M-1}\lambda_j}\right] + \frac{1}{2}l(2M-l)\log N, \tag{33}$$

where $l \in \{0, 1, \ldots, M-1\}$. The MDL channel order estimate is

$$\hat{L} = \underset{l}{\operatorname{argmin}}\ \mathrm{MDL}\,(l)\,. \tag{34}$$

2) EFFICIENT CHANNEL ORDER DETERMINATION METHOD

The ECOD method estimates the channel order by utilizing the ratio of two consecutive eigenvalues and can be computed as [26]

$$\mathrm{ECOD}\,(l) = \begin{cases} \dfrac{\lambda_l}{\lambda_{l-1} - 2\lambda_l} & \text{when } l > 0 \text{ and } \lambda_l \leq \dfrac{\lambda_{l-1}}{3}, \\ 1 & \text{otherwise,} \end{cases} \tag{35}$$

where $l \in \{0, 1, \ldots, M-1\}$. The ECOD channel order estimate is

$$\hat{L} = \underset{l}{\operatorname{argmin}}\ \mathrm{ECOD}\,(l)\,. \tag{36}$$

D. PATH SELECTION CRITERION FOR CHANNEL ORDER OVERESTIMATION

The MDL method may overestimate the channel order that can cause the ESPRIT algorithm to produce delay outliers in the form of the false paths arriving before the true earliest path [18], [21], [24]. To avoid the impact of the delay outliers on positioning, the proposed ESPRIT discriminator applies a path selection criterion.

Before defining the criterion, the effect of the channel order overestimation on the ESPRIT delay output is studied. For this purpose, the proposed discriminator is coupled with the MDL and simulated in the AWGN channel without multipath in 10^5 realizations. The evaluation is performed using the CSI-RS pilots of the 5G NR downlink evaluation waveform from Section II-A. The ESPRIT design parameter is set to $m = 0.24$ resulting in $M = \lfloor 819 \cdot 0.24 \rfloor = 196$ eigenvalues. The estimated delay $\hat{\tau}_0$ and $\hat{\mathrm{SNR}}_0$ of the earliest path in each channel realization are shown for the evaluated SNR equal to 12 dB and -6 dB in Figs. 4a and 4b, respectively. The SNR of the l-th path is estimated as

$$\hat{\mathrm{SNR}}_l = 10 \log_{10} \left(\frac{P\,|\hat{\Lambda}_l|^2}{\hat{\mathbf{w}}^H \hat{\mathbf{w}}} \right) [\mathrm{dB}], \tag{37}$$

where $\hat{\mathbf{w}}$ is the noise vector estimated using the complex amplitudes in (31) as $\hat{\mathbf{w}} = \hat{\mathbf{h}} - \hat{\mathbf{G}}\,\hat{\mathbf{\Lambda}}$.

Figs. 4a and 4b show that the MDL method may indeed overestimate the channel order as values $\hat{L} = 2$ and $\hat{L} = 3$ are observed. The overestimations may result in false earliest paths that are characterized by large negative delays and low SNRs, both of which are unrelated to the SNR of the overall signal. Although the negative delay outliers only appear when the channel order is overestimated, the overestimation itself does not always lead to negative delay outliers.

To remove the false earliest paths and allow the usage of the MDL for positioning, Driusso *et al.* [20] applied a filtering threshold to the ESPRIT delay measurements, exploiting their large negative values. However, this approach requires estimation of the delay and its confidence margin, and might miss the small negative values. Figs. 4a and 4b show that instead of the delay measurements, the false earliest paths can be filtered based on their SNRs as these remain low for both large and small negative delays.

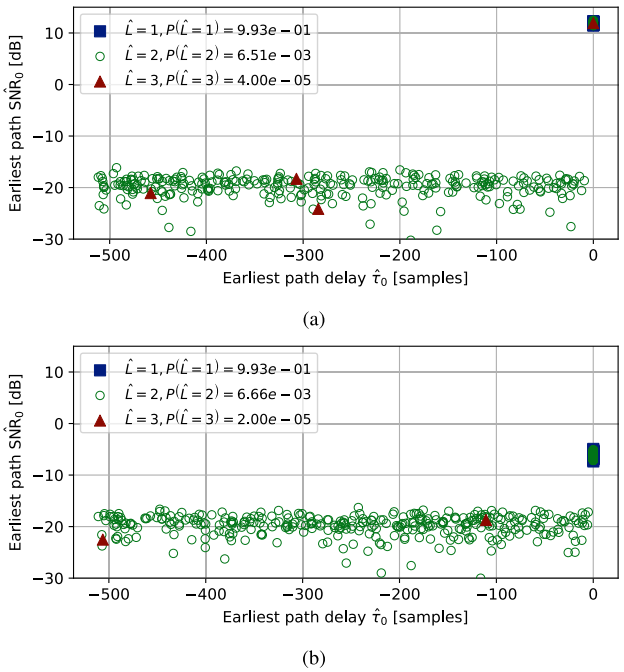

FIGURE 4. Delay and SNR of the earliest path estimated by the ESPRIT algorithm in each channel realization for the SNR equal to (a) 12 dB and (b) −6 dB. The value of the channel order $\hat{L}$ estimated by the MDL in a given realization is indicated by the marker style. The probability of occurrence of a given channel order $P(\hat{L})$ is also shown.

The proposed path selection criterion selects the earliest path whose SNR exceeds a configurable threshold γ [dB]. Using the estimated SNR from (37), the index of the earliest path l_γ exceeding the threshold is determined as

$$l_\gamma = \underset{l}{\operatorname{argmin}}\{\hat{\mathrm{SNR}}_l > \gamma\}. \tag{38}$$

The proposed ESPRIT discriminator uses the l_γ-th path to determine the delay offset from (27) as

$$D^{(\tau)}_{\mathrm{ESPRIT}} = \hat{\tau}_{l_\gamma}, \tag{39}$$

and the phase offset from (32) as

$$D^{(\phi)}_{\mathrm{ESPRIT}} = \hat{\phi}_{l_\gamma}. \tag{40}$$

The threshold γ can be derived empirically using the results of the outlier analysis of the discriminator outputs for a given configuration and various SNRs. The threshold depends on the number of pilots P and configured data snapshot size M. Since the outliers are well distinguishable in the evaluation shown in Fig. 4, the threshold is set to be 6 dB above the maximum SNR of the outlier paths (-16 dB) resulting in $\gamma = -10$ dB. Although this threshold may also potentially discard a very weak LOS component, signals with

such low SNRs are not expected to be tracked in practical positioning scenarios.

V. PERFORMANCE OF JOINT DELAY AND PHASE DISCRIMINATOR BASED ON ESPRIT

The performance of the proposed joint delay and phase discriminator based on ESPRIT coupled with the MDL and ECOD methods is studied. The discriminator is evaluated in two configurations. In the first configuration, denoted as ESPRIT, no path selection criterion is applied to neither MDL nor ECOD and the resulting discriminators are referred to as ESPRIT/MDL and ESPRIT/ECOD. In the second configuration, denoted as ESPRIT-S, a path selection threshold $\gamma = -10$ dB derived from the results of Section IV-D is applied to the MDL method. The resulting discriminator is referred to as ESPRIT-S/MDL. No path selection is performed for the ECOD. The EMLP delay and ATAN2 phase discriminators are considered as references in the study. Delay and phase errors are estimated by tracking the CSI-RS pilots of the 5G NR waveform from Section II-A. The ESPRIT design parameter is set to $m = 0.24$ resulting in data snapshots of length $M = \lfloor 819 \cdot 0.24 \rfloor = 196$ providing a sufficient multipath resolution for the simulations. The correlator spacing of the EMLP discriminator is set to $\delta = 0.1$. The received signal power is assumed to be perfectly known at the receiver.

A. DELAY TRACKING THRESHOLD AND COMPUTATION COMPLEXITY

The delay tracking thresholds ζ of the ESPRIT and EMLP discriminators are determined using (28) and (11), respectively. To derive ζ_{EMLP}, a linearity threshold $\alpha = 0.05$ is assumed. The results summarized in Table 2 show that the ESPRIT discriminator has three orders of magnitude larger tracking threshold than the EMLP. Such a large threshold allows to either reduce the update rate of the tracking loop or to track delay offsets with high variances without causing the tracking loop to lose the lock of the signal.

The main drawback of the ESPRIT discriminator is its computational complexity that is higher than that of the EMLP due to numerous matrix operations involving inversion, singular value decomposition, and eigenvalue computation [24]. To evaluate the computational overhead, the average times needed to process the CSI-RS pilots of a single slot of the 5G NR evaluation waveform are measured. The algorithms are implemented in the Python programming language and executed in a computer running the Intel Core i5 processor at 2.4 GHz. Table 2 shows that ESPRIT requires three orders of magnitude more processing time than the EMLP. The processing time of the ESPRIT discriminator (97.11 ms) is in this implementation also much larger than the duration of the 5G radio slot (0.5 ms). This limits the real-time usage of ESPRIT in the receivers if a high loop update rate is desired. However, given that the ESPRIT discriminator provides a large delay tracking threshold, the update rate might be reduced. The performance of the algorithm could also be optimized with tailored hardware and software.

TABLE 2. Delay tracking thresholds ζ and processing times of the ESPRIT and EMLP discriminators.

Discriminator	ζ [sample]	ζ [μs]	Processing time [ms]
ESPRIT	512.00	4.17	97.11
EMLP$_{\delta=0.1}$	0.317	0.0027	0.08

B. DELAY AND PHASE ERRORS IN ABSENCE OF MULTIPATH

The delay and phase errors of the discriminators are studied in the AWGN channel in the absence of multipath. This evaluation helps to understand the performance of the discriminators in the multipath-free environment and study the lower bounds of the errors. In the case of the delay error, the results are compared to the CRLB in (10). The evaluated SNR ranges from -18 dB to 18 dB. Although the SNR range goes lower than the expected values in a vicinity of a cell, it helps to understand the performance limits of the discriminators and generalize the results. Each discriminator is simulated 10^4 times for a given SNR. For comparison, the ESPRIT discriminator fixed to the true number of paths ($\hat{L} = 1$) is used in the evaluation. The standard deviations of delay and phase errors of the evaluated discriminators are shown in Figs. 5a and 5b, respectively. The non-zero probabilities of the channel orders estimated by the MDL and ECOD methods are shown in Figs. 6a and 6b, respectively. Values reported as $\hat{L} = 0$ indicate that the estimator is unable to identify any path and that ESPRIT produces neither delay nor phase outputs.

The standard deviation of the delay error of the ESPRIT discriminator fixed to the true number of paths approaches the CRLB for the SNR above -12 dB as shown in Fig. 5a. Fig. 5b shows a similar behavior of the phase error of the ESPRIT discriminator fixed to the true number of paths as it approaches the ATAN2 discriminator representing the lower bound of the error.

Figs. 5a and 5b show that the standard deviations of neither delay nor phase errors of the ESPRIT/MDL discriminator approach the CRLB or ATAN2. This is due to the presence of the delay outliers studied in Section IV-D. The MDL method overestimates the channel order with values as high as $\hat{L} = 3$ regardless of the SNR as shown in Fig. 6. When using the MDL, taking the ESPRIT delay and phase outputs without applying a path selection criterion is not recommended for positioning.

The ESPRIT-S/MDL discriminator employing the proposed path selection criterion from Section IV-D correctly removes the phase and delay outliers of the ESPRIT/MDL as the standard deviations of the delay and phase errors converge to the CRLB and ATAN2 for the SNR above -12 dB as shown in Figs. 5a and 5b. The ESPRIT-S/MDL discriminator does not produce any estimates for the SNR below -12 dB as no paths above the configured threshold $\gamma = -10$ dB are detected. This is not considered a problem as the removed estimates are in the SNR range in which the performance of the ESPRIT discriminator fixed to the true

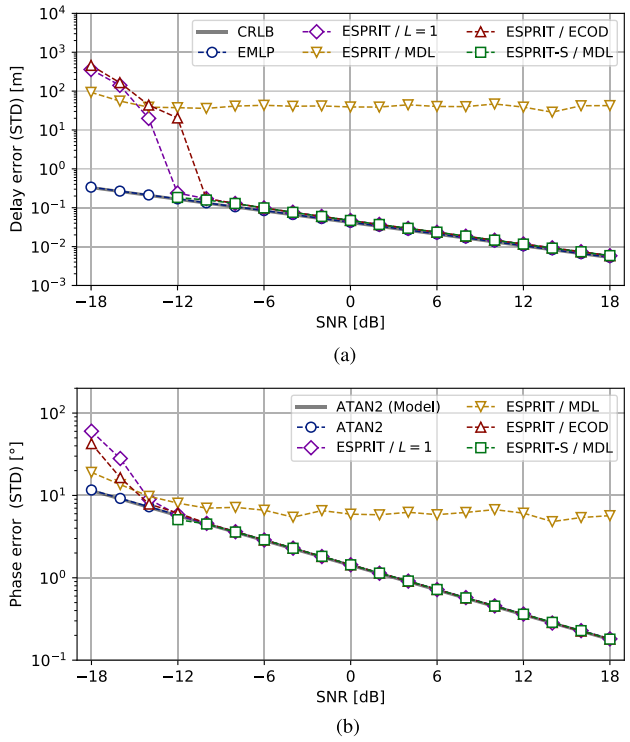

FIGURE 5. Standard deviations of the (a) delay and (b) phase errors of the evaluated discriminators in the AWGN channel without multipath. The ESPRIT-S/MDL discriminator with the path selection criterion does not produce any delay or phase estimates for the SNR below −12 dB as no paths above the configured SNR threshold $\gamma = -10$ dB are detected.

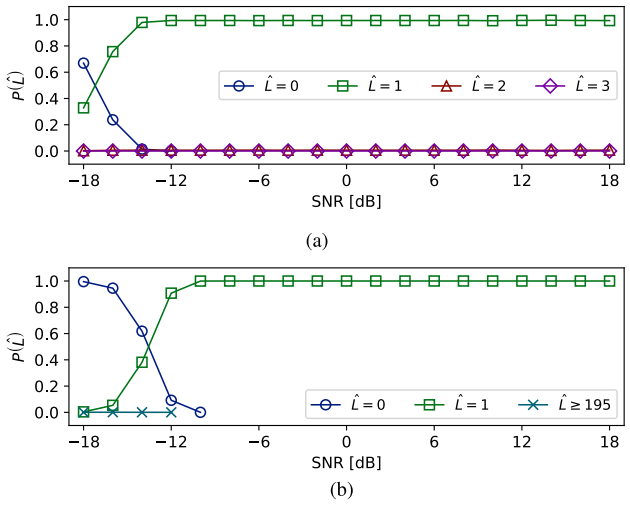

FIGURE 6. Probabilities of the channel orders estimated by the (a) MDL and (b) ECOD methods in the AWGN channel without multipath. The channel orders with zero probabilities are not shown to identify when no channel with that order is detected. For example, the ECOD method does not produce any estimates of $\hat{L} = 0$ for the SNR above −10 dB.

number of paths does not approach the CRLB and ATAN2 anyways.

Figs. 5a and 5b show that the standard deviations of the delay and phase errors of the ESPRIT/ECOD discriminator also converge to the CRLB and ATAN2 for the SNR above −12 dB. Fig. 6b shows that although the ECOD method may overestimate the channel order for the SNR below −10 dB by identifying the majority of eigenvalues as signal components ($\hat{L} \geq 195$), the method remains stable in a sufficiently high SNR. The path selection criterion is not needed by ESPRIT when the ECOD is used.

C. DELAY AND PHASE ERRORS IN PRESENCE OF MULTIPATH

To study the delay and phase errors of the discriminators in the presence of multipath, a multipath error envelope is evaluated by simulating a two-ray channel model containing the LOS component and a single reflection. Although the two-ray channel is a very particular model, its use is widely accepted by the GNSS community as a generally representative way to assess the robustness and sensitivity of a given estimator to multipath. Likewise, in the case of 5G NR positioning, this model is specific but beneficial to generally understand the fundamental impact of a single path on the discriminator performance. The power of the reflected path is configured to −3 dB of the power of the LOS component. The excess path delay ranges from 0 to 3 samples. In the delay error evaluation, the phase of the reflection is set to 0 rad and π rad corresponding to constructive and destructive multipath combination, respectively. In the phase error evaluation, the phase of the reflection is set to $\pm\frac{3}{4}\pi$ rad. The multipath error envelope of the EMLP and ATAN2 discriminators is usually evaluated in a noiseless channel as the mean error is independent of the noise. However, this cannot be done with the ESPRIT discriminator as the channel order estimation depends on the SNR. As such, the mean and root-mean-square (RMS) of the delay and phase errors are evaluated in the SNR equal to 12 dB. Due to the unsatisfactory performance of the ESPRIT/MDL discriminator in the AWGN channel without multipath presented in Section V-B, the MDL without the path selection criterion is not considered in this evaluation.

The observed multipath delay error envelopes of the EMLP, ESPRIT/ECOD, and ESPRIT-S/MDL discriminators are shown in Fig. 7a. The related root-mean-square delay errors are shown in Fig. 7b. The observed multipath phase error envelopes of the ATAN2, ESPRIT/ECOD, and ESPRIT-S/MDL discriminators are shown in Fig. 8a. The related root-mean-square phase errors are shown in Fig. 8b.

Fig. 7a shows that the ESPRIT/ECOD and ESPRIT-S/MDL delay discriminators perform similarly to the EMLP for small multipath excess delays. Above a given multipath excess delay, the ESPRIT discriminators start resolving the reflection in the channel and the mean delay errors rapidly converge to zero in both constructive and destructive cases, achieving better performances than the EMLP. Fig. 7b shows that the root-mean-square delay errors of both ESPRIT discriminators also converge to very small values once a given multipath excess delay is reached.

Similar to the delay errors, the mean phase errors of the ESPRIT/ECOD and ESPRIT-S/MDL rapidly converge

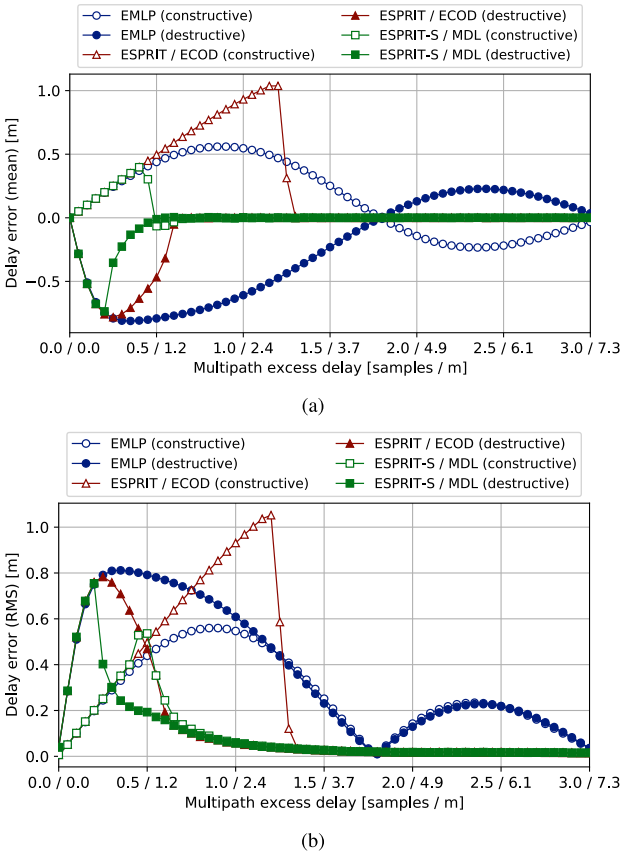

FIGURE 7. (a) Mean delay errors and (b) root-mean-square delay errors of the evaluated discriminators in the two-ray channel model.

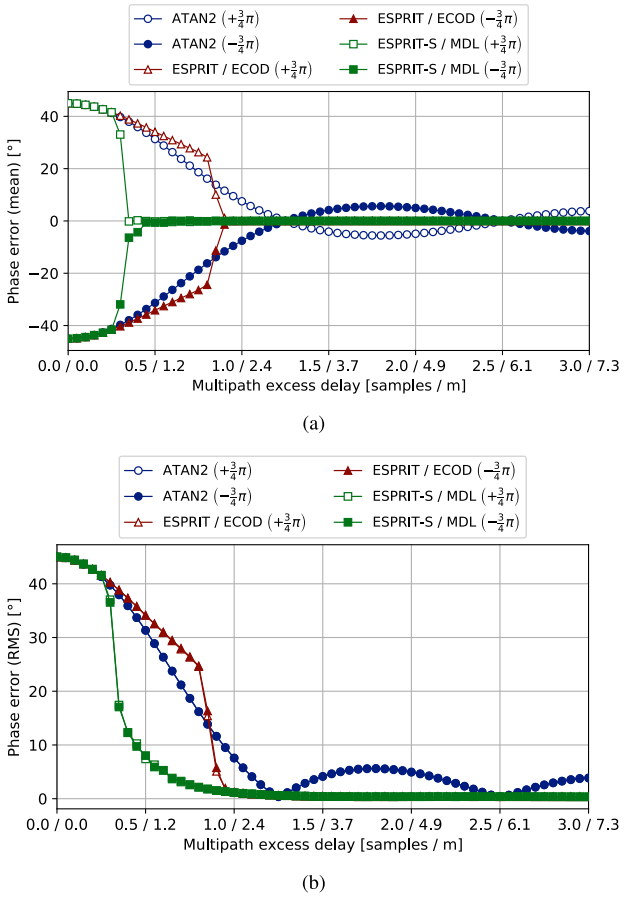

FIGURE 8. (a) Mean phase errors and (b) root-mean-square phase errors of the evaluated discriminators in the two-ray channel model.

to zero above a given multipath excess delay as shown in Fig. 8a, outperforming the ATAN2 discriminator. The ESPRIT-S/MDL discriminator achieves lower root-mean-square phase errors than the ATAN2 as shown in Fig. 8b.

The convergence of the mean delay and phase errors to zero occurs for the ESPRIT-S/MDL discriminator at a noticeably smaller excess delay than for the ESPRIT/ECOD as shown in Figs. 7a and 8a. To understand the convergence, the mean delay error of the ESPRIT-S/MDL is shown in Fig. 9a for the constructive multipath for the excess delay between 0.40 and 0.54 samples. The related non-zero probabilities of the total number of paths above the SNR threshold (L_γ) outputted by the discriminator are shown in Fig. 9b. It can be seen that the convergence of the mean delay error to zero coincides with the increasing probability of resolving the reflection ($L_\gamma = 2$). To describe the convergence, the multipath resolution τ_{MR} is defined as the multipath excess delay at which the probability of resolving all the paths in the channel is $P(L_\gamma = 2) = 0.5$. For example, the MDL method achieves a multipath resolution of $\tau_{\mathrm{MR}} = 0.470$ samples for the SNR equal to 12 dB as shown in Fig. 9b.

To compare the multipath resolution of the MDL and ECOD, τ_{MR} of both channel order methods is evaluated for the SNR ranging from 6 dB to 18 dB. The results obtained for constructive and destructive multipath are shown in Fig. 10. The MDL method achieves a better multipath resolution than the ECOD in both cases, explaining the lower multipath excess delay needed for the convergence of the delay and phase errors in the case of the ESPRIT-S/MDL shown in Figs. 7 and 8. The ESPRIT-S/MDL discriminator provides superior performance for positioning than the ESPRIT/ECOD.

D. DELAY AND PHASE ERRORS IN TERRESTRIAL 3GPP CHANNEL MODEL

The evaluation of the delay and phase errors of the discriminators in a realistic terrestrial 5G NR multipath environment is performed using the 3GPP TDL-E channel model containing 14 taps [31]. The Rician K-factor is set to $K = 0$ dB retaining half of the power of the signal in the multipath components. The channel is generated 10^4 times. In each channel realization, the phase of each tap is randomly generated following a uniform distribution $\varphi \sim U(-\pi, \pi)$. The SNR is set to 12 dB. The root-mean-square delay and phase errors are evaluated for the values of the delay spread (DS) between 20 ns and 200 ns. The DS is used to scale the normalized path delays from the TDL-E model to obtain the desired multipath excess delays. The data snapshot length of the ESPRIT discriminator ($M = 196$) is considered sufficient

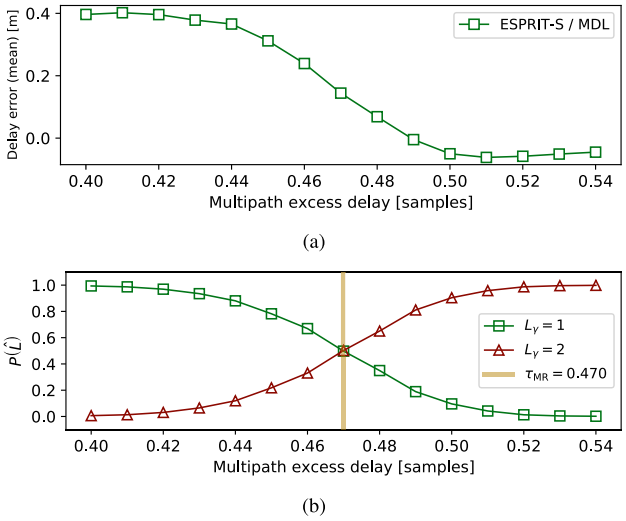

FIGURE 9. (a) Mean delay errors of the ESPRIT-S/MDL discriminator; and (b) associated non-zero probabilities of the estimated total number of paths above the SNR threshold.

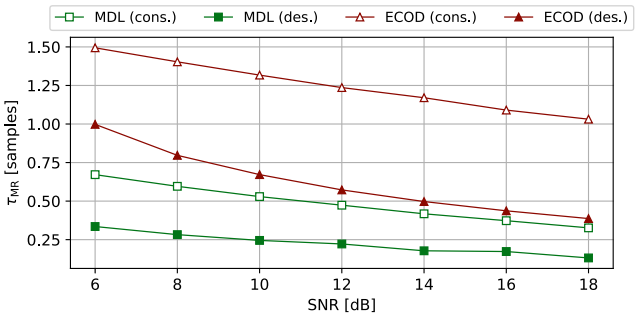

FIGURE 10. Multipath resolutions of the MDL and ECOD methods in the two-ray channel model.

to estimate the $L = 14$ signal components present in the channel. The root-mean-square delay and phase errors of the discriminators are shown in Figs. 11a and 11b, respectively.

Figs. 11a and 11b show that the proposed ESPRIT-S/MDL discriminator achieves lower root-mean-square delay and phase errors than the EMLP and ATAN2 discriminators for all evaluated delay spreads. The exception is the phase error for a very low delay spread of DS = 20 ns as shown in Fig. 11b, where the ESPRIT-S/MDL discriminator remains more biased than the ATAN2. This is attributed to a very small path separation preventing the ESPRIT algorithm to properly distinguish the paths in the channel. The ESPRIT-S/MDL achieves noticeably better performance in a realistic multipath environment than the traditionally used EMLP and ATAN2 discriminators.

E. COMPARISON OF 5G NR AND LTE

The performance of the ESPRIT discriminator in 5G NR is compared to the previous generation of cellular signals in the AWGN channel in the absence and presence of multipath. In the case of LTE, the CRS pilots of the LTE downlink evaluation waveform from Section II-B are tracked.

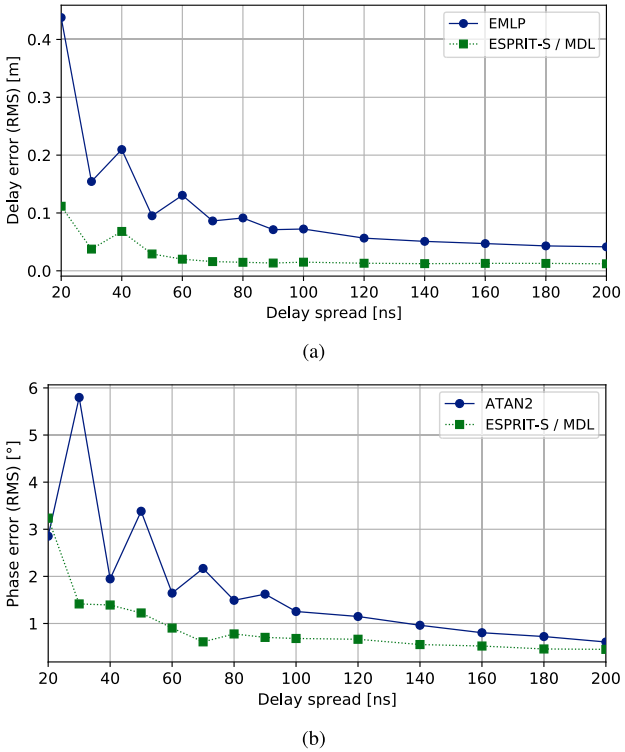

FIGURE 11. Root-mean-square (a) delay and (b) phase errors of the evaluated discriminators in the 3GPP TDL-E channel model.

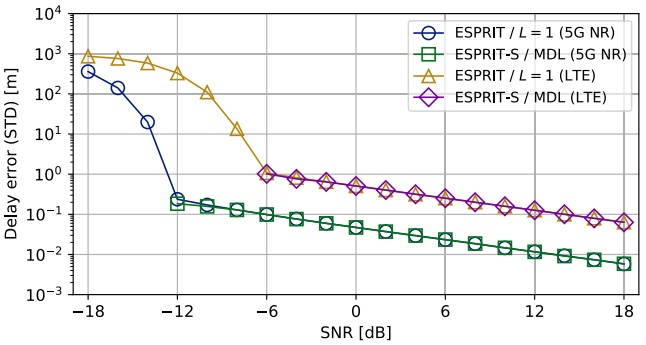

FIGURE 12. Standard deviations of the delay errors of the ESPRIT-S/MDL discriminator tracking the 5G NR and LTE evaluation waveforms in the AWGN channel. The standard deviations of the delay errors of the ESPRIT discriminator fixed to the true number of paths are also shown.

The path selection threshold of the ESPRIT-S/MDL is set to $\gamma = -3$ dB and the ESPRIT design parameter is set to $m = 0.48$ resulting in data snapshots of length $M = \lfloor 200 \cdot 0.48 \rfloor = 96$. The standard deviations of the delay errors of the ESPRIT-S/MDL in the AWGN channel without multipath are shown in Fig. 12. The mean delay errors of the ESPRIT-S/MDL observed in the two-ray channel model are shown in Fig. 13 for the SNR equal to 12 dB.

Fig. 12 shows that the discriminators achieve an order of magnitude better standard deviation of the delay error in 5G NR than in LTE when no multipath is present. The tracking is also possible for a lower SNR in 5G NR. Fig. 13 shows a better performance of 5G NR in the two-ray channel model as it achieves a sub-meter delay error. Better performances in

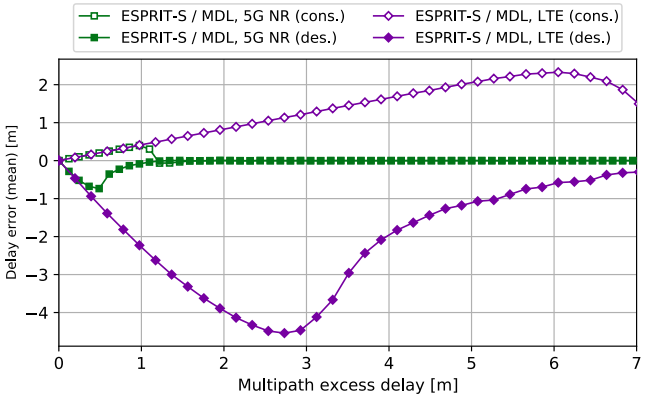

FIGURE 13. Mean delay errors of the ESPRIT-S/MDL discriminator tracking the 5G NR and LTE evaluation waveforms in the two-ray channel model.

both scenarios are obtained thanks to the higher number of available pilots and higher signal bandwidth.

VI. CONCLUSION

A joint delay and phase discriminator based on ESPRIT was proposed for positioning with 5G NR downlink cellular signals. The study of the effect of the MDL channel order overestimation on the ESPRIT algorithm led to the introduction of the path selection criterion based on the SNR. The ESPRIT-S/MDL discriminator with the path selection criterion eliminates the delay and phase outliers produced by the ESPRIT/MDL without the criterion, confirming its suitability for positioning purposes. The ESPRIT-S/MDL achieves lower mean and root-mean-square delay and phase errors than the EMLP and ATAN2 discriminators in the presence of multipath in the two-ray channel model after a given multipath excess delay. The ESPRIT-S/MDL also achieves lower root-mean-square delay and phase errors in a representative 5G channel model. The higher computational complexity of the ESPRIT algorithm could be optimized with tailored hardware and software. Although the algorithm is proposed for implementations inside the signal tracking loops, the presented results remain valid for open-loop and snapshot implementations.

REFERENCES

[1] *Study on NR Positioning Support*, document TR 38.855, 3GPP, Mar. 2019.

[2] E. Kaplan and C. Hegarty, *Understanding GPS/GNSS: Principles and Applications*, 3rd ed. Norwood, MA, USA: Artech House, 2017.

[3] C. Mensing, S. Sand, and A. Dammann, "Hybrid data fusion and tracking for positioning with GNSS and 3GPP-LTE," *Int. J. Navigat. Observ.*, vol. 2010, pp. 1–12, Aug. 2010.

[4] G. De Angelis, G. Baruffa, and S. Cacopardi, "GNSS/cellular hybrid positioning system for mobile users in urban scenarios," *IEEE Trans. Intell. Transp. Syst.*, vol. 14, no. 1, pp. 313–321, Mar. 2013.

[5] J. A. Del Peral-Rosado, R. E. I Castillo, J. Miguez-Sanchez, M. Navarro-Gallardo, J. A. Garcia-Molina, J. A. López-Salcedo, G. Seco-Granados, F. Zanier, and M. Crisci, "Performance analysis of hybrid GNSS and LTE Localization in urban scenarios," in *Proc. 8th ESA Workshop Satell. Navigat. Technol. Eur. Workshop GNSS Signals Signal Process. (NAVITEC)*, Noordwijk, The Netherlands, Dec. 2016, pp. 1–8.

[6] J. A. Del Peral-Rosado, R. E. I Castillo, J. A. López-Salcedo, G. Seco-Granados, Z. Chaloupka, L. Ries, and J. A. Garcia-Molina, "Evaluation of hybrid positioning scenarios for autonomous vehicle applications," in *Proc. ION GNSS*, Portland, OR, USA, Sep. 2017, pp. 2541–2553.

[7] G. Destino, J. Saloranta, G. Seco-Granados, and H. Wymeersch, "Performance analysis of hybrid 5G-GNSS localization," in *Proc. 52nd Asilomar Conf. Signals, Syst., Comput.*, Pacific Grove, CA, USA, Oct. 2018, pp. 8–12.

[8] K. Shamaei and Z. M. Kassas, "Sub-meter accurate UAV navigation and cycle slip detection with LTE carrier phase measurements," in *Proc. 32nd Int. Tech. Meeting Satell. Division Inst. Navigat.*, Miami, FL, USA, Oct. 2019, pp. 2469–2479.

[9] *NR: Physical Channels and Modulation*, document TS 38.211, 3GPP, Dec. 2020.

[10] *Evolved Universal Terrestrial Radio Access (E-UTRA): Physical Channels and Modulation*, document TS 36.211, 3GPP, Dec. 2020.

[11] W. Xu, M. Huang, C. Zhu, and A. Dammann, "Maximum likelihood TOA and OTDOA estimation with first arriving path detection for 3GPP LTE system," *Trans. Emerg. Telecommun. Technol.*, vol. 27, no. 3, pp. 339–356, Mar. 2016.

[12] K. Shamaei, J. Khalife, and Z. M. Kassas, "Comparative results for positioning with secondary synchronization signal versus cell specific reference signal in LTE systems," in *Proc. Int. Tech. Meeting Conf.*, Monterey, CA, USA, Jan. 2017, pp. 1256–1268.

[13] H. Asplund, D. Astely, P. von Butovitsch, T. Chapman, M. Frenne, F. Ghasemzadeh, M. Hagström, B. Hogan, G. Jöngren, J. Karlsson, F. Kronestedt, and E. Larsson, "3GPP physical layer solutions for NR," in *Advanced Antenna Systems for 5G Network Deployments*, H. Asplund, D. Astely, P. von Butovitsch, T. Chapman, M. Frenne, F. Ghasemzadeh, M. Hagström, B. Hogan, G. Jöngren, J. Karlsson, F. Kronestedt, and E. Larsson, Eds. New York, NY, USA: Academic, 2020, pp. 351–422. [Online]. Available: https://www.sciencedirect.com/science/article/pii/B9780128200469000095

[14] B. Yang, K. B. Letaief, R. S. Cheng, and Z. Cao, "Timing recovery for OFDM transmission," *IEEE J. Sel. Areas Commun.*, vol. 18, no. 11, pp. 2278–2291, Nov. 2000.

[15] D. Serant, P. Thevenon, M.-L. Boucheret, O. Julien, C. Macabiau, S. Corazza, M. Dervin, and L. Ries, "Development and validation of an OFDM/DVB-T sensor for positioning," in *Proc. IEEE/ION Position, Location Navigat. Symp.*, Indian Wells, CA, USA, May 2010, pp. 988–1001.

[16] L. Chen, P. Thevenon, G. Seco-Granados, O. Julien, and H. Kuusniemi, "Analysis on the TOA tracking with DVB-T signals for positioning," *IEEE Trans. Broadcast.*, vol. 62, no. 4, pp. 957–961, Dec. 2016.

[17] J. A. del Peral-Rosado, J. A. Lopez-Salcedo, G. Seco-Granados, F. Zanier, P. Crosta, R. Ioannides, and M. Crisci, "Software-defined radio LTE positioning receiver towards future hybrid localization systems," in *Proc. 31st AIAA Int. Commun. Satell. Syst. Conf.*, Florence, Italy, Oct. 2013, pp. 1–11.

[18] K. Shamaei and Z. M. Kassas, "LTE receiver design and multipath analysis for navigation in urban environments," *Navigat., J. Inst. Navigat.*, vol. 65, no. 4, pp. 655–675, Dec. 2018.

[19] X. Li and K. Pahlavan, "Super-resolution TOA estimation with diversity for indoor geolocation," *IEEE Trans. Wireless Commun.*, vol. 3, no. 1, pp. 224–234, Jan. 2004.

[20] M. Driusso, F. Babich, F. Knutti, M. Sabathy, and C. Marshall, "Estimation and tracking of LTE signals time of arrival in a mobile multipath environment," in *Proc. 9th Int. Symp. Image Signal Process. Anal. (ISPA)*, Zagreb, Croatia, Sep. 2015, pp. 276–281.

[21] M. Driusso, F. Babich, F. Knutti, M. Sabathy, H. Mathis, and C. Marshall, "Vehicular position tracking using LTE signals," *IEEE Trans. Veh. Technol.*, vol. 66, no. 4, pp. 3376–3391, Apr. 2017.

[22] H. Dun, C. C. J. M. Tiberius, and G. J. M. Janssen, "Positioning in a multipath channel using OFDM signals with carrier phase tracking," *IEEE Access*, vol. 8, pp. 13011–13028, 2020.

[23] M. Wax and T. Kailath, "Detection of signals by information theoretic criteria," *IEEE Trans. Acoust., Speech, Signal Process.*, vol. ASSP-33, no. 2, pp. 387–392, Apr. 1985.

[24] P. Wang and Y. J. Morton, "Performance comparison of time-of-arrival estimation techniques for LTE signals in realistic multipath propagation channels," *Navigation*, vol. 67, no. 4, pp. 691–712, Dec. 2020.

[25] A. P. Liavas and P. A. Regalia, "On the behavior of information theoretic criteria for model order selection," *IEEE Trans. Signal Process.*, vol. 49, no. 8, pp. 1689–1695, Aug. 2001.

[26] A. P. Liavas, P. A. Regalia, and J.-P. Delmas, "Blind channel approximation: Effective channel order determination," *IEEE Trans. Signal Process.*, vol. 47, no. 12, pp. 3336–3344, 1999.

[27] *NR: Base Station (BS) Radio Transmission and Reception*, document TS 38.104 V17.0.0, 3GPP, Dec. 2020.

[28] *NR: Physical Layer Procedures for Control*, document TS 38.213, 3GPP, Dec. 2020.
[29] *Evolved Universal Terrestrial Radio Access (E-UTRA); Base Station (BS) radio transmission and reception*, document TS 36.104, 3GPP, Dec. 2020.
[30] J. A. Del Peral-Rosado, J. A. López-Salcedo, G. Seco-Granados, F. Zanier, and M. Crisci, "Achievable localization accuracy of the positioning reference signal of 3GPP LTE," in *Proc. Int. Conf. Localization*, Starnberg, Germany, Jun. 2012, pp. 1–6.
[31] *NR: Study on Channel Model for Frequencies From 0.5 to 100 GHz*, document TR 38.901, 3GPP, Dec. 2019.

IVAN LAPIN received the M.Sc. and Ph.D. degrees in telecommunications from the Slovak University of Technology in Bratislava, Slovakia. He joined the European Space Agency (ESA), as an EGNOS System Performance Engineer, in 2016. He is currently a Research Fellow with ESA working on hybrid GNSS/5G positioning and integrity. His main research interests include 5G and GNSS signal processing, software-defined radios, impact of ionospheric scintillation on GNSS receivers, and performances of navigation systems.

GONZALO SECO-GRANADOS (Senior Member, IEEE) received the Ph.D. degree in telecommunications engineering from the Universitat Politecnica de Catalunya, Spain, in 2000, and the M.B.A. degree from the IESE Business School, Spain, in 2002. From 2002 to 2005, he was a member of the European Space Agency, where he was involved in the design of the Galileo system and receivers. In 2015 and 2019, he was a Fulbright Visiting Scholar at the University of California at Irvine, Irvine, CA, USA. He is currently a Professor with the Department of Telecommunication, Universitat Autonoma de Barcelona, where he worked as the Vice Dean of the Engineering School, from 2011 to 2019. His research interests include localization based on GNSS and 5G systems. Since 2018, he has been serving as a member for the Sensor Array and Multichannel Technical Committee for the IEEE Signal Processing Society. Since 2019, he has been the President of the Spanish Chapter of the IEEE Aerospace and Electronic Systems Society.

OLIVIER RENAUDIN received the M.Sc. degree in electrical engineering from the École Nationale Supérieure d'Electronique, Informatique et Radiocommunications de Bordeaux (ENSEIRB), Université Bordeaux 1, in 2006, and the Ph.D. degree in electrical engineering from the Université Catholique de Louvain (UCLouvain), in 2013. From 2014 to 2016, he was a Postdoctoral Researcher with the University of Southern California (USC). He is currently a Postdoctoral Researcher with the Universitat Autònoma de Barcelona (UAB). His research interests include wireless channel measurement and modeling for vehicle-to-vehicle and 5G communication systems, parameter estimation, and signal processing with applications to communications and navigation.

FRANCESCA ZANIER received the M.Sc. degree in telecommunications engineering and the Ph.D. degree from the University of Pisa, Italy. She joined the European Space Agency, ESTEC, Noordwijk, The Netherlands, in 2009, where she is currently a Radio Navigation System Engineer with the Radio Navigation Systems and Techniques Section of the Technical Directorate. Her research interests include signal processing, estimation theory, GNSS receivers, and signals and navigation applications.

LIONEL RIES is currently the Head of the Radio Navigation Systems and Techniques Section, Directorate of Technology, Engineering and Quality, ESA, the European Space Agency. He joined ESA, as a Radio Navigation System Engineer, in 2016, supporting activities on future navigation systems and concepts (both at infrastructure and user segment level) as well as on standardization of 5G positioning in 3GPP. Beforehand, he worked with CNES (French Space Agency), first supporting GNSS-related research and development activities and European Commission on Galileo, then leading CNES Section for localization/navigation signal and equipment.